

# Journal of Biomedical Optics

BiomedicalOptics.SPIEDigitalLibrary.org

## **Pancreatic cancer cell detection by targeted lipid microbubbles and multiphoton imaging**

Benjamin Cromey  
Ashley McDaniel  
Terry Matsunaga  
Josef Vagner  
Khanh Quoc Kieu  
Bhaskar Banerjee

**SPIE.**

Benjamin Cromey, Ashley McDaniel, Terry Matsunaga, Josef Vagner, Khanh Quoc Kieu, Bhaskar Banerjee,  
“Pancreatic cancer cell detection by targeted lipid microbubbles and multiphoton imaging,” *J.*  
*Biomed. Opt.* **23**(4), 046501 (2018), doi: 10.1117/1.JBO.23.4.046501.

# Pancreatic cancer cell detection by targeted lipid microbubbles and multiphoton imaging

Benjamin Cromey,<sup>a,\*</sup> Ashley McDaniel,<sup>b</sup> Terry Matsunaga,<sup>b,c</sup> Josef Vagner,<sup>d</sup> Khanh Quoc Kieu,<sup>a</sup> and Bhaskar Banerjee<sup>b,c,e</sup>

<sup>a</sup>University of Arizona, College of Optical Sciences, Tucson, Arizona, United States

<sup>b</sup>University of Arizona, College of Medicine, Department of Medical Imaging, Tucson, Arizona, United States

<sup>c</sup>University of Arizona, Department of Biomedical Engineering, Tucson, Arizona, United States

<sup>d</sup>University of Arizona, BIO5 Institute, Ligand Discovery Laboratory, Tucson, Arizona, United States

<sup>e</sup>University of Arizona, College of Medicine, Department of Medicine, Tucson, Arizona, United States

**Abstract.** Surgical resection of pancreatic cancer represents the only chance of cure and long-term survival in this common disease. Unfortunately, determination of a cancer-free margin at surgery is based on one or two tiny frozen section biopsies, which is far from ideal. Not surprisingly, cancer is usually left behind and is responsible for metastatic disease. We demonstrate a method of receptor-targeted imaging using peptide ligands, lipid microbubbles, and multiphoton microscopy that could lead to a fast and accurate way of examining the entire cut surface during surgery. Using a plectin-targeted microbubble, we performed a blinded *in-vitro* study to demonstrate avid binding of targeted microbubbles to pancreatic cancer cells but not noncancerous cell lines. Further work should lead to a much-needed point-of-care diagnostic test for determining clean margins in oncologic surgery. © 2018 Society of Photo-Optical Instrumentation Engineers (SPIE) [DOI: 10.1117/1.JBO.23.4.046501]

Keywords: multiphoton; cancer research; pancreatic cancer; nonlinear optics; targeted microbubbles; in-vitro testing.

Paper 170811R received Dec. 19, 2017; accepted for publication Mar. 13, 2018; published online Apr. 9, 2018.

## 1 Introduction

Pancreatic cancer is the 10th most common cancer in men and women in the United States yet is the 4th highest cause of cancer death.<sup>1</sup> Pancreatic resection is the only chance of cure for the 20% of patients who are candidates for surgery and involves removal of the head (Whipple's resection) or tail of the pancreas.<sup>2</sup> Unfortunately, this extensive and time-consuming surgery is far from perfect, and the flaw is in leaving behind residual cancer tissue, which is the strongest independent risk factor of poor survival.<sup>3-7</sup> During surgery, a soft, normal area of the pancreas is palpated at the neck of the pancreas to guide resection. One or two biopsies are then taken from the pancreatic duct at the surface of the excised specimen for frozen section microscopy. Although this process oftentimes fails to sample more than 1% of the resected surface, it is the sole determinant of adequate resection during surgery. Several days after surgery, when formal pathology is completed, cancer is often found at the margin, but it is too late to conduct a second operation.<sup>5</sup>

Postsurgically, the macro- and microscopic assessments of the entire specimen determine if the surgical margin is truly free of cancer (R0) or cancer is found within 1 mm of a margin (R1).<sup>4</sup> The presence of an R0 margin is associated with double the survival of R1 margins.<sup>6-8</sup> Following a rigorous postsurgery histopathologic examination of resected tissue, no patient with an R1 margin survived beyond 24 months, whereas 80% of those with R0 margins were alive almost 5 years later; no other clinical or pathological variable affected survival.<sup>5,7</sup> Clearly, new methods are needed to help identify and remove all unseen cancer and improve survival in this devastating disease.

Lipid microbubbles decorated with antibodies or peptide ligands targeted to cell surface receptors can be used to identify diseased tissue with high sensitivity and specificity.<sup>9</sup> Microbubbles are traditionally detected by ultrasound, but the requirement of a contact medium (ultrasound gel) between the transducer and the bubbles at the tissue surface may cause the bubbles to collapse and burst.<sup>10-12</sup> Our earlier preliminary work had demonstrated the utility of multiphoton microscopy (MPM) in detecting microbubbles on cell surfaces without the need for a contact medium.<sup>13</sup> The multiphoton microscope is becoming increasingly important in biological studies because of its ability to see contrast inherent to tissue without the need for external stains.<sup>14,15</sup> We have been using a lab-designed multiphoton microscope for several years for various applications.<sup>16-18</sup> Recently, we have demonstrated that the bubbles can be detected via third-harmonic generation (THG) using our microscope.<sup>13</sup> This paper continues that work to demonstrate the capability of these targeted microbubbles to aid in the determination of cancerous versus normal pancreatic cells *in vitro* and to assess its feasibility as a diagnostic tool.

## 2 Methodology

### 2.1 Cell Description

Human pancreatic cancer PANC1 cells were purchased from the American Type Culture Collection (ATCC; CRL1469) and grown in Dulbecco's Modified Eagle Medium (DMEM) with 4.5-g/L glucose, L-glutamine, and sodium pyruvate supplemented with 10% fetal bovine serum and 1% penicillin-streptomycin. Human pancreatic hTERT-HPNE cells were purchased from ATCC (CRL4023) and grown in DMEM media with 4.5-g/L

\*Address all correspondence to: Benjamin Cromey, E-mail: [bcromey@email.arizona.edu](mailto:bcromey@email.arizona.edu)

glucose, L-glutamine, and sodium pyruvate supplemented with 10% fetal bovine serum, 1% penicillin–streptomycin, and VEGF growth kit (ATCC; PCS100041). Immortalized PANC1 cells between 80 and 100 passages and primary hTERT-HPNE cells between 8 and 15 passages were used in the experiments. The PANC1s usually reached 90% to 100% confluency while the hTERT-HPNEs were about 50% confluent.

## 2.2 Microbubbles Description

Because of the overexpression of plectin-1 (Plec1) receptors in pancreatic cancer cells (PANC1), a peptide ligand was developed and added to the microbubble formulation to selectively target the Plec1 receptor.<sup>13,19</sup> To make the targeting ligand, a peptide was covalently attached to the bis-palmitoyl lipid-like moiety via a short polyethyleneglycol spacer (extended span distance 140 Å). The specific peptide sequence was Lys – Thr – Leu – Leu – Pro – Thr – Pro – NH<sub>2</sub>. The synthesis of the bioconjugate ligand was performed by solid-phase technology using a Fmoc/tBu protection strategy. The structure and the microbubbles are shown in Fig. 1.

The composition used for the control microbubbles was 2 mol. % DDPE-PEG 2000 and 98 mol. % DPPC dispersed in a propylene glycol, normal saline, glycerol solution (15:80:5, v:v:v). The composition used for the Plec1 targeted bubbles was 2 mol. % of the targeting ligand and 98 mol. % DPPC similarly dispersed in the propylene glycol, normal saline, and glycerol solution (15:8:5, v:v:v). In addition, when needed, 0.2% concentration 1,1'-dioctadecyl-3,3,3',3'-tetramethylindocarbocyanine perchlorate (DiI, Thermo Fisher, Carlsbad, California) ( $E_{x,max} = 549$  nm and  $E_{m,max} = 565$  nm) was added as a fluorescent label. The total lipid concentration in all formulations was 1 mg/mL and the solution was aliquoted in 1.5-mL increments into 2-mL glass vials, sealed with air-tight septums, and followed by purging with perfluorobutane gas

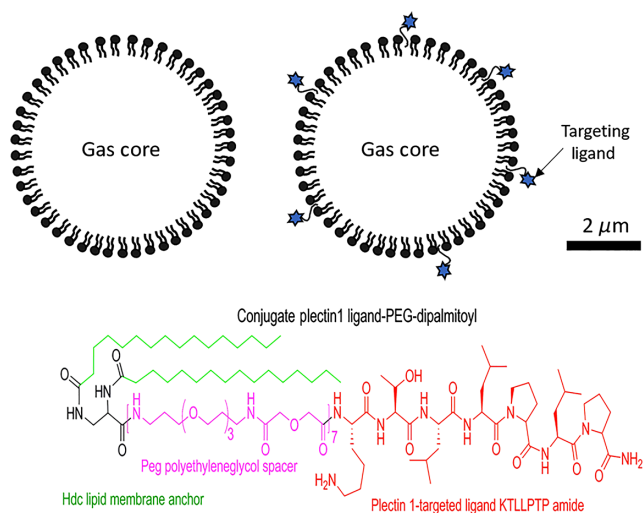


**Fig. 1** Targeted microbubbles (top left) were made with the ligand seen below it. Control bubbles (top right) were identical except lacking the targeting ligand. The diameter of the microbubbles generally ranged between 1 and 5  $\mu$ m. The ligand used was a Plec1 lipid-like bioconjugate. The Plec1 peptide ligand is covalently bound via an amide linkage to a PEGylated spander followed by linkage to diamino butyrate and two palmitoyl fatty acids. The lipid-like end inserts into the membrane to form a targeted microbubble as demonstrated previously.<sup>20</sup>

(FluoroMed LP, Round Rock, Texas). The vial was then agitated using a modified dental amalgamator (Lantheus, New York, New York) to form the microbubbles used in imaging.

## 2.3 Sample Preparation

Cells were seeded onto poly-D-lysine-coated glass bottomed dishes (MatTek, Ashland, Massachusetts) ~24 h prior to imaging in order to ensure adherence. To prepare the cells for imaging, cells were incubated for 5 min with 5-mL media and stained with 5- $\mu$ L Calcein AM (Thermo Fisher Scientific, Carlsbad, California), followed by additional media and 200  $\mu$ L of DiI microbubbles (0.2% concentration). The media cocktail was added to completely fill the dish and parafilm was used to seal it. Due to the buoyancy of the bubbles, the dish was inverted so the bubbles would be in contact with the cells. After incubating with microbubbles for 20 min, the dishes were rinsed twice with Dulbecco's phosphate-buffered saline to remove any debris or unbound bubbles from the dish. DMEM media was then reintroduced to the dish during imaging. The fluorescent labels, Calcein AM and DiI, were used to confirm microbubbles binding to live cells in the two-photon excitation channel. Coregistration of microbubbles would be confirmed independently by two-photon excitation of the fluorescent labels and the THG signals of the microbubbles. The Calcein AM label, in addition to insuring cell viability, would also provide background contrast in the images to clearly indicate that the microbubbles were binding to the surface of the cells and not to the plate surface.

## 2.4 Imaging and Microscope Description

Our multiphoton microscope was designed and built in-house<sup>21</sup> and is controlled by Labview-based software developed in our research group. A schematic overview of the microscope system is shown in Fig. 2. We used a compact femtosecond fiber laser as the excitation light source. Since MPM is a point imaging technique, a pair of galvanometric scan mirrors was used to raster the laser beam in both X- and Y-dimensions. A collimated laser beam was presented to this raster scanner, after which the beam was expanded to fill the back aperture of the objective. An afocal pair of lenses is used to expand the laser beam by approximately

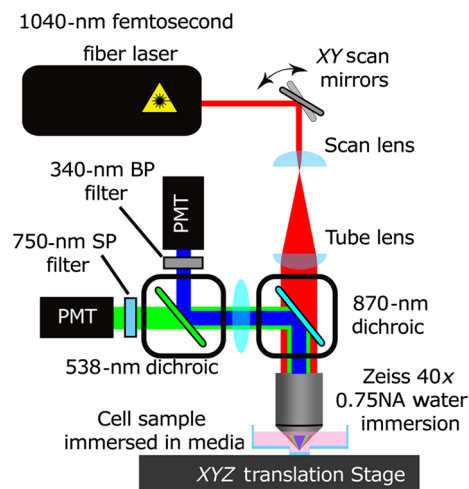


**Fig. 2** Schematic of lab-built multiphoton microscope, configured for this project.

a factor of 4. This telescope setup also served to relay the scan mirror image onto the back aperture of the objective, ensuring that all the scan angles were supported by the imaging system without vignetting.

For this study, we imaged with a 1040-nm femtosecond fiber laser as the illumination source. The Zeiss Achromplan 40× 0.75 numerical aperture (NA) water-immersion microscope objective was used to image the samples. The signal light returning from the sample was split into two channels by a 538-nm longpass dichroic mirror (Semrock), detected by Hamamatsu H-10721 Photomultiplier Tubes, and their signal amplified with Stanford Research SR570 preamplifiers. The transmitted channel had a 750-nm shortpass filter to remove any remaining 1040-nm light from reaching the detector, allowing the detection of two-photon-excited fluorescence (2PEF). The reflected channel had a 340-nm bandpass filter with a 22-nm full width at half maximum pass window to isolate the THG signal.

## 2.5 Blinded Study Methodology

Four sets of experiments (one experimental and three controls) were conducted using the following in order to investigate the selectivity of the targeted microbubbles: (1) PANC1 incubated with targeted microbubbles (experimental), (2) PANC1 incubated with nontargeted microbubbles (control), (3) noncancerous ductal epithelial pancreatic cells (hTERT) incubated with targeted microbubbles (control), and (4) noncancerous pancreatic cells incubated with nontargeted microbubbles (control). Each set of experiments was performed at least 10 times to confirm the accuracy of the results. When imaging the cells, the researcher who performed the multiphoton imaging task was blinded as to which microbubbles were used in the sample being imaged in order to eliminate bias when observing and analyzing the images.

## 2.6 Statistical Approach

In order to create a more quantitative assessment of the number of bubbles in each cell dish, we define a bubble index

$$\text{Bubble index} = \frac{\text{number of bubbles in image}}{\text{number of cells in image}} \quad (1)$$

This bubble index was computed for every cell dish. For each image captured from a dish, an individual bubble index was found by counting the number of bubbles and the number

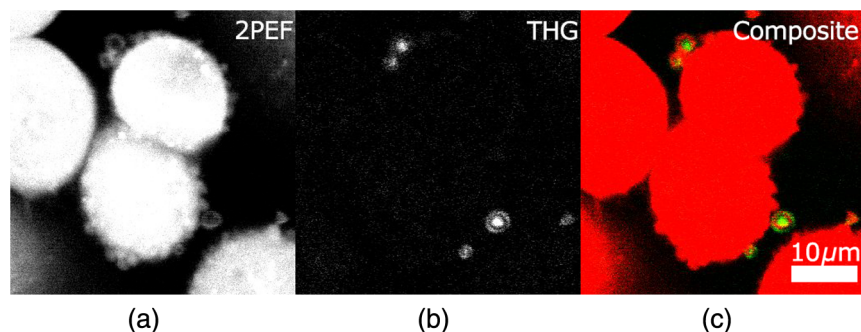
of cells that were 75% or more visible in the field of view regardless of whether microbubbles were adherent to those cells. Some basic statistics would then be used to analyze the results. First, the bubble index would be averaged across all the images taken in one cell dish. Then, each of these averages would be averaged across all of the dishes used in each group of the study. We could then do a hypothesis test on the mean for each experiment using the standard *t*-test in statistics. To use this, we had to set our null hypothesis, or the guess as to what the mean would be that we would like our experiment to disprove. Since we hoped to see a bubble index larger than one for only the experimental group, we set the null hypothesis to be that all experiments would have a bubble index of zero. This would mean that all experiments showed no binding by the targeted bubbles. This *t*-test would be applied to the average bubble index for each set of experiments and reported with the average. The *t*-test reports a *p*-value, which indicates the probability of the reported mean occurring given the null hypothesis. A small *p*-value would indicate our results had statistical significance.

## 3 Imaging Results

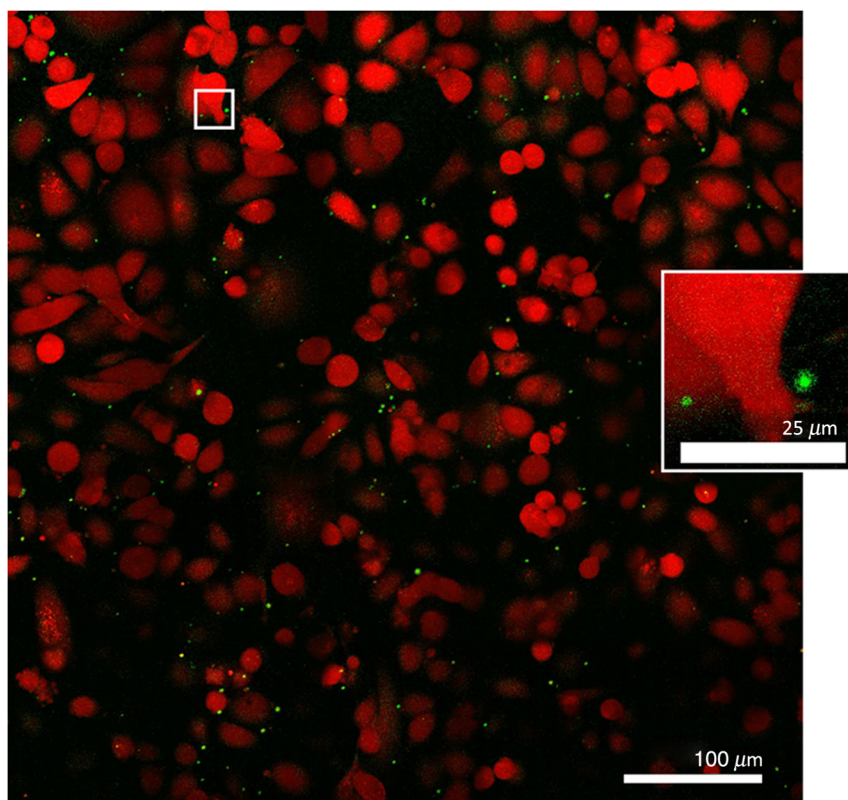
The described four experiments were performed in over 20 imaging sessions over the course of a year, removing the possibility of the cell targeting being a one-time effect. The images were recorded by our software and analyzed using the Fiji<sup>22</sup> release of ImageJ.<sup>23</sup> False color was added to overlay the two signals, captured as intensity grayscale images, with 2PEF colored in red and THG colored in green. Small amounts of processing were performed on the captured images, including balancing the brightness of the two channels and decreasing the background noise.

Figure 3 highlights the different information received from each channel. In the 2PEF channel, a signal is detected both from the calcein inside of the cells and from the DiI that labeled the microbubble membrane. In the THG channel, the signal is predominantly received from the bubbles themselves. THG is generated by the bubbles as a result of the third order nonlinearity ( $\chi_3$ ) mismatch between the liquid media, the bubble membrane, and the gas inside the bubbles.<sup>13</sup>

A large stitched<sup>24</sup> image of cancerous cells with targeted bubbles can be seen in Fig. 4. The green color represents THG, which highlights the bubbles. The red color originates from the 2PEF emission from the calcein dye-stained cells. There are several bubbles that appear to be by themselves instead of being attached to a cell, but we are confident that they are attached to



**Fig. 3** (a) A grayscale image of only 2PEF, (b) THG signal from the same location, and (c) a composite image with both signals overlaid with false color. The 2PEF image is deliberately overexposed so that the weaker DiI signal from the bubbles can be seen.



**Fig. 4** Stitched image of cancerous cells with targeted bubbles. This stitched image is  $575\ \mu\text{m} \times 575\ \mu\text{m}$ . The green images seen are microbubbles highlighted with THG. An inset shows a closer view of what an individual bubble looks like to the microscope. This image has a bubble index of 0.66.

a cell outside of the depth of field. Cell dishes were always investigated at multiple image depths to look for bubbles. Due to the nature of multiphoton imaging, out-of-focus cells do not produce the signal, so that we do not detect the cells beneath the plane of a single focal position. The depth of focus of the imaging configuration used for much of this study was calculated to be  $2.46\ \mu\text{m}$ , based on our  $0.75\ \text{NA}$  objective and the  $1040\text{-nm}$  wavelength. This is smaller than the  $5\text{-}\mu\text{m}$  average size of an individual bubble, showing that it is possible for the bubble above a cell to be seen and not the cell itself. The lateral resolution of our imaging system for THG can be calculated to be  $400\ \text{nm}$ , based on the wavelength and objective used.<sup>25,26</sup>

Since the MPM only detects the signal near focus, depth-resolved images could be captured by acquiring pictures at different  $z$  locations of the same region of interest (commonly referred to as  $z$ -stacks in microscopy). These could be rendered into a three-dimensional (3-D) reconstruction of the sample using the 3-D viewer functionality in Fiji.<sup>27</sup> Figure 5 is an example, taken by imaging the same cells increasing in depth by  $1\ \mu\text{m}$  among images. Figure 5 is  $125\text{-}\mu\text{m} \times 125\text{-}\mu\text{m}$  wide and  $30\text{-}\mu\text{m}$  deep and shows the bright green microbubbles adhering to the tops and sides of several cells. Green background can also be seen from the THG signal generated by the bottom of the dish near the bottom cells.

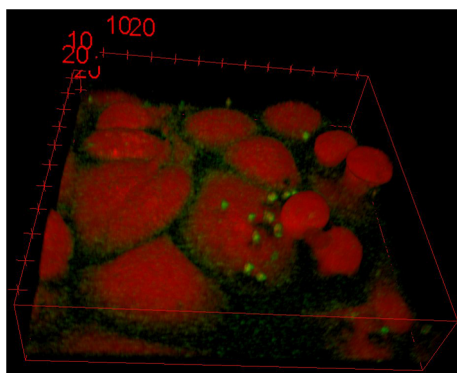


**Fig. 5** Three-dimensional rendering made via the Fiji 3-D viewer plugin. The green objects are bubbles. The rendering is  $125\text{-}\mu\text{m} \times 125\text{-}\mu\text{m}$  wide and  $30\text{-}\mu\text{m}$  deep.

## 4 Results Discussion

At least 10 experiments were collected for each sample set. In 100% of the instances, based upon the amount of bubbles binding or lack thereof, the researcher who performed the imaging task was able to accurately distinguish the experimental group from the control groups. A more detailed description of each experiment is contained in Tables 2 and 3 in the Appendix. As described previously, two sets of averages were taken from each experimental group. The average bubble index of each cell dish for each experiment was computed, and binned into a histogram displayed in Fig. 6. Most of the data sets fall near zero, whereas the experimental group is mostly removed from the other sets. Additionally, the bubble index was averaged across all the cell dishes for each experiment, leading to a final average shown in the inset of Fig. 6.

The final averages of each data set and the  $p$ -value from the statistical analysis are reported in Table 1. The goal was to see a

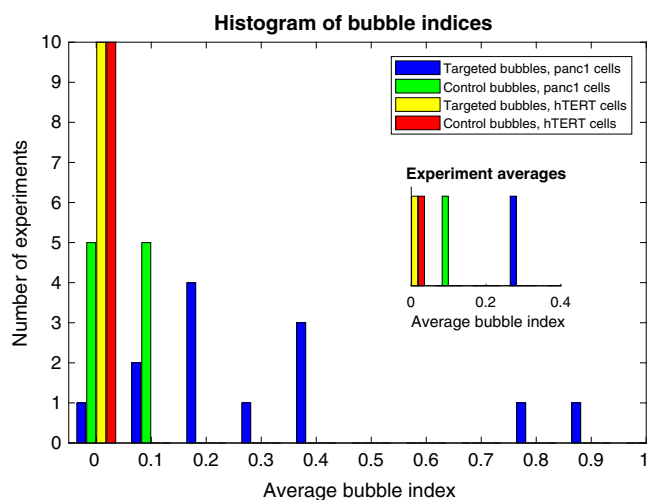


**Fig. 6** A histogram of average bubble indices for each individual data set. Inset: the average of each individual experiment group.

**Table 1** Average bubble index and  $p$ -value for each experiment.

Experiment	Bubble index	Ratio to experimental group	$P$ -value
PANC1 with targeted bubbles	0.3300	1.00	0.0006
PANC1 with control bubbles	0.0542	6.08	0.0152
hTERT with targeted bubbles	0.0030	110.0	0.1689
hTERT with control bubbles	0.0011	300.0	0.1852

$p$ -value of  $<0.01$  to report significance. The  $p$ -value for the targeted bubbles and PANC1 cells clearly meet this criterion at a value of 0.0006.

The most important experiment comparison comes between the two targeted bubble data sets, because this determines whether or not this method is useful to detect cancer cells. We see that the bubbles occurred on average 110 times more in the cancer cell group than the healthy cell group.

We also see in the table that the bubble index for the experimental group is around six times larger than the next closest control group. When the control bubbles and PANC1 cells experiments were being examined, images were usually only captured when a bubble was seen, even though most of the sample did not have bubbles. As a result of this image capture methodology, the bubble index for that experiment is skewed higher, making it a worst-case comparison. A comparative test on the mean between the control and targeted PANC1's also shows that the difference between them is also significant with  $p = .0116$ . The control bubble experiments were performed to ensure that the bubbles were binding to the receptors targeted by the ligand and not for some other reason.

A summary of the image results can be seen in Fig. 7. The only location that bubbles were seen in high frequency was when the bubbles were targeted and in contact with cancerous cells.

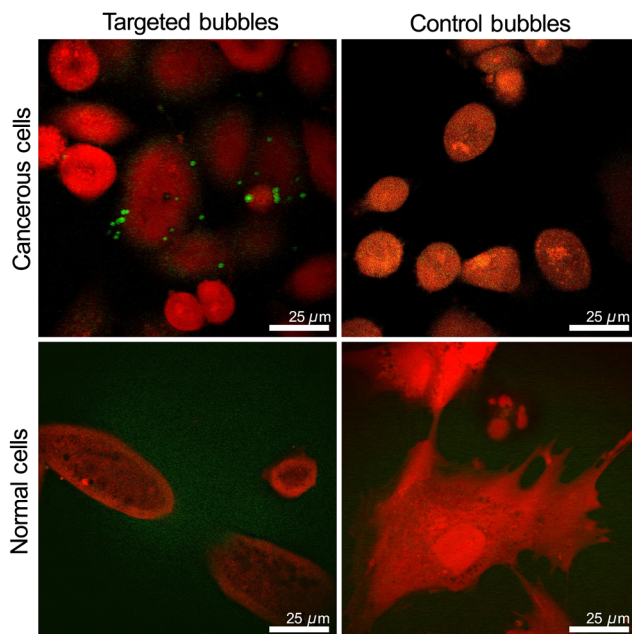


**Fig. 7** This matrix of representative images highlights the results of the study. The majority of the time bubbles were detected, seen in green, was when the bubbles were targeted bubbles in the cancer cell dishes. The green background in the normal cell images came from THG signal from the interface of the bottom of the dish and the liquid media.

#### 4.1 False Positives

It is noted that the targeting ligand for the microbubbles is highly selective; however, there is always the possibility of nonspecific binding to noncancerous cells. The possibility for bubbles to be trapped in tightly packed cells also leads to the chance for control bubbles to be seen in the cancerous cells. During our experiments, we occasionally saw microbubbles in small numbers binding in one of the three control experiments. We also discovered that it was possible for the bubbles to adhere to the bottom of the tray of the hTERT cells due to the poly-D-lysine coating at the bottom of the tray, leading to a few false positives. However, these bubbles were isolated in pockets of cells or adherent to the bottom of the cell culture plate. These effects were reduced by identifying only those microbubbles bound over the calcein background or directly on the fringe of the calcein fluorescence (i.e., a cell edge).

Proof of these results is shown in Fig. 8, where Fig. 8(a) shows hTERT cells with targeted bubbles, Fig. 8(b) shows PANC1 cells with targeted bubbles, and Fig. 8(c) shows a region in a targeted dish of hTERT cells with no cells in the field of view.

The difference could be seen in the distance between the bubbles between the two groups. In the inset for each cell set, it could be seen how the cells bound directly to the cells in the PANC1 set, as they appeared adjacent to the membrane. By contrast, the bubbles in the hTERT appeared 10  $\mu\text{m}$  or more from the cells themselves, indicating they could not be binding to the cells, and must be adhering to the poly-D-lysine coating. As shown in Fig. 8(c), bubbles could even be occasionally found sticking to the poly-D-lysine coating with no cells present. Because this condition only exists in this experimental setting, this would probably not be an issue in a clinical setting. These bubbles were not counted for computing the bubble index for that set of images, because they were not binding to the cell itself.

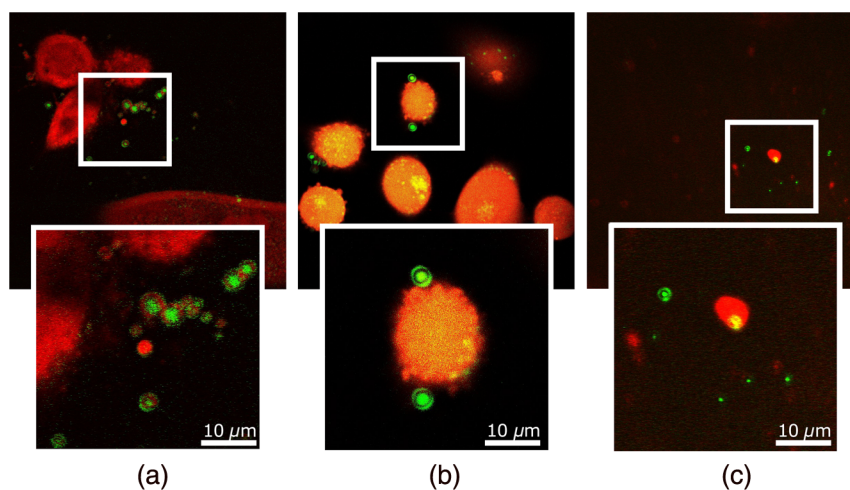


**Fig. 8** (a) hTERT cells and targeted bubbles. (b) PANC1 cells and targeted bubbles. The bubbles bind directly to the cells in the PANC1 cells, as they appear next to the membrane. The bubbles in the hTERT dish were almost  $10\ \mu\text{m}$  away from the cell membrane. (c) Bubbles seen sticking to the poly-D-lysine coating with no cells present.

## 4.2 Discussion

The long-term focus of this project is to design a point-of-care methodology that can determine a cancer-free resection using targeted microbubbles. Because it is possible to miniaturize a multiphoton into a probe form factor,<sup>28</sup> these bubbles could be imaged in a surgical setting, allowing the physician to rapidly determine whether the resected margins are indeed cancer free. In addition, we have previously demonstrated the use of second-harmonic generation and THG as a method of label-free cancer determination in Barrett's esophagus and ovarian cancer.<sup>16,17</sup> We plan to combine these two methods in the future to gather information both about the surface of a sample with the bubbles and potentially up to 1-mm deep through tissue to examine beneath the surgical margin. By adding the capability for a physician to look deeper through tissue, we believe that we can further increase confidence that the cancerous tissue has been removed, thereby increasing the probability of long-term survival of the patient. As an intermediate step, we will evaluate this technique in identifying cancer in samples of pancreatic tissue.

## 4.3 Conclusion

In this study, we demonstrated a method of identifying cancerous cell lines using peptide ligands, lipid microbubbles, and MPM. We believe that this could lead to a fast and accurate method for examining the entire cut surface during surgery. This is in sharp contrast to the current state of the art, where long surgery times and small sampling area make survival less likely. We found on average that the bubbles appeared over 100 times more often in the cancerous cells compared to the healthy cells. Throughout the study, the bubbles bound to the cancer cells in higher frequency across the entire sample surface, clearly separating it from the noncancerous cell lines, which only occasionally showed bubbles in a few locations.

## Appendix: Complete List of Experiments and Results

This appendix provides a complete list of the experiments performed in this study. Tables 2 and 3 includes the experiment

**Table 2** Experiment list and results comments.

Date	Dish number	Cell type	Bubble type	Bubble index	Comments
October 26, 2016	1	PANC1	Targeted	2.042	Not blinded to give researcher practice in finding bubbles. These results are excluded from our averages.
	2	PANC1	Targeted	0.896	
November 9, 2016	1	PANC1	Targeted	0.383	Blinded study begins
	2	PANC1	Control	0.099	
November 30, 2016	1	PANC1	Control	0.056	
	2	PANC1	Targeted	0.321	
December 7, 2016	1	PANC1	Targeted	0.243	
	2	PANC1	Control	0.126	
	3	PANC1	Targeted	0.190	

**Table 2** (Continued).

Date	Dish number	Cell type	Bubble type	Bubble index	Comments
January 25, 2017	1	PANC1	Control	0.000	hTERTs not very confluent
	2	PANC1	Targeted	0.150	
	1	hTERT	Targeted	0.000	
	2	hTERT	Control	0.000	
February 1, 2017	1	PANC1	Targeted	0.363	Fig. 8(b)
	2	PANC1	Control	0.148	Top right of Fig. 7
	3	PANC1	Targeted	0.000	Dish sat out for longer time: lack of bubbles could be function of binding time
	4	PANC1	Control	0.000	
February 15, 2017	1	PANC1	Targeted	0.189	Tested 25x immersion lens
	2	PANC1	Control	0.011	
February 22, 2017	1	PANC1	Targeted	0.387	
	2	PANC1	Control	0.089	
	3	PANC1	Targeted	0.219	
	4	PANC1	Control	0.013	
March 1, 2017	1	hTERT	Targeted	0.111	Fig. 8(a)
	2	hTERT	Control	0.000	
March 8, 2017	1	hTERT	Targeted	0.000	
	2	hTERT	Control	0.000	
	3	PANC1	Targeted	0.136	
	4	PANC1	Control	0.000	
March 22, 2017	1	hTERT	Targeted	0.000	Bottom left of Fig. 7
	2	hTERT	Control	0.000	

**Table 3** Experiment list and results comments, continued

Date	Dish number	Cell type	Bubble type	Bubble index	Comments
July 6, 2017	1	hTERT	Targeted	0.000	
	2	hTERT	Targeted	0.016	
	3	hTERT	Control	0.000	
	4	hTERT	Control	0.007	
July 7, 2017	1	hTERT	Targeted	0.000	
	2	hTERT	Targeted	0.000	
	3	hTERT	Control	0.004	
	4	hTERT	Control	0.000	
July 12, 2017	1	hTERT	Targeted	0.014	Bottom right of Fig. 7
	4	hTERT	Control	0.000	
August 17, 2017	1	PANC1	Targeted	0.933	Figs. 3 and 4
	2	PANC1	Targeted	0.776	Fig. 5
September 14, 2017	1	hTERT	Targeted	0.000	Fig. 8(c)
	2	hTERT	Targeted	0.000	

group, the bubble index, and any comments on the details of the experiment.

### Disclosures

The authors declare no conflicts of interest.

### Acknowledgments

The authors would like to thank Katha Patel and Phuong-Trinh Dao of the Medical Student Research Program [No. R25NS076437 (KP and PT)] for assistance in sample and bubble preparation. We thank R. Dawson Baker for numerous useful discussions on data analysis. Funding for this project came from the National Science Foundation (NSF) Graduate Research Fellowship under Grant No. DGE-1143953 and NSF Electrical, Computer and Cyber Systems (ECCS) under Grant No. ECCS-1610048.

### References

- R. L. Siegel, K. D. Miller, and A. Jemal, "Cancer statistics, 2017," *CA Cancer J. Clin.* **67**(1), 7–30 (2017).
- C. J. Wray et al., "Surgery for pancreatic cancer: recent controversies and current practice," *Gastroenterology* **128**(6), 1626–1641 (2005).
- G. Benassai et al., "Factors influencing survival after resection for ductal adenocarcinoma of the head of the pancreas," *J. Surg. Oncol.* **73**(4), 212–218 (2000).
- K. Kato et al., "Prognostic factors for survival after extended pancreatectomy for pancreatic head cancer: influence of resection margin status on survival," *Pancreas* **38**(6), 605–612 (2009).
- K. V. Menon et al., "Impact of margin status on survival following pancreatoduodenectomy for cancer: the Leeds pathology protocol (LEEPP)," *HPB* **11**, 18–24 (2009).
- C. P. Raut et al., "Diagnostic accuracy of endoscopic ultrasound-guided fine-needle aspiration in patients with presumed pancreatic cancer," *J. Gastrointest. Surg.* **7**, 118–128 (2003).
- C. P. Raut et al., "Impact of resection status on pattern of failure and survival after pancreatoduodenectomy for pancreatic adenocarcinoma," *Ann. Surg.* **246**(1), 52–60 (2007).
- I. Esposito et al., "Most pancreatic cancer resections are R1 resections," *Ann. Surg. Oncol.* **15**, 1651–1660 (2008).
- T. O. Matsunaga et al., "Phase-change nanoparticles using highly volatile perfluorocarbons: toward a platform for extravascular ultrasound imaging," *Theranostics* **2**, 1185–1198 (2012).
- J. Castle and S. B. Feinstein, *Drug and Gene Delivery Using Sonoporation for Cardiovascular Disease*, pp. 331–338, Springer International Publishing, Cham (2016).
- E. Unger et al., "Cardiovascular drug delivery with ultrasound and microbubbles," *Adv. Drug Delivery Rev.* **72**(Suppl. C), 110–126 (2014).
- T. R. Porter, S. A. Choudhury, and F. Xie, "Utilization of diagnostic ultrasound and intravenous lipid-encapsulated perfluorocarbons in non-invasive targeted cardiovascular therapeutics," *J. Ther. Ultrasound* **4**, 18 (2016).
- K. Harpel et al., "Imaging of targeted lipid microbubbles to detect cancer cells using third harmonic generation microscopy," *Biomed. Opt. Express* **7**, 2849–2860 (2016).
- K. König, "Multiphoton microscopy in life sciences," *J. Microsc.* **200**(2), 83–104 (2000).
- W. R. Zipfel, R. M. Williams, and W. W. Webb, "Nonlinear magic: multiphoton microscopy in the biosciences," *Nat. Biotech.* **21**, 1369–1377 (2003).
- J. K. Barton et al., "Three-photon imaging of ovarian cancer," *Proc. SPIE* **9689**, 96893P (2016).
- S. Mehra et al., "Label-free multi-photon imaging of dysplasia in Barrett's esophagus," *Biomed. Opt. Express* **7**, 148–157 (2016).
- L. Karvonen et al., "Rapid visualization of grain boundaries in monolayer MoS<sub>2</sub> by multiphoton microscopy," *Nat. Commun.* **8**, 15714 (2017).
- D. Bausch et al., "Plectin-1 as a novel biomarker for pancreatic cancer," *Clin. Cancer Res.* **17**, 302–309 (2011).
- P. A. Schumann et al., "Targeted-microbubble binding selectively to GPIIb/IIIa receptors of platelet thrombi," *Invest. Radiol.* **37**(11), 587–593 (2002).
- K. Kieu et al., "Label-free multi-photon imaging using a compact femtosecond fiber laser mode-locked by carbon nanotube saturable absorber," *Biomed. Opt. Express* **4**, 2187–2195 (2013).
- J. Schindelin et al., "Fiji—an open source platform for biological image analysis," *Nat. Methods* **9**, 676–682 (2012).
- C. A. Schneider, W. S. Rasband, and K. W. Eliceiri, "NIH image to ImageJ: 25 years of image analysis," *Nat. Methods* **9**, 671–675 (2012).
- S. Preibisch, S. Saalfeld, and P. Tomancak, "Globally optimal stitching of tiled 3D microscopic image acquisitions," *Bioinformatics* **25**(11), 1463–1465 (2010).
- B. R. Masters and P. So, *Handbook of Biomedical Nonlinear Optical Microscopy*, Oxford University Press, New York (2008).
- M. Gu, "Resolution in three-photon fluorescence scanning microscopy," *Opt. Lett.* **21**, 988–990 (1996).
- B. Schmid et al., "A high-level 3D visualization API for Java and ImageJ," *BMC Bioinf.* **11**, 274 (2010).
- G. Liu et al., "Multiphoton microscopy system with a compact fiber-based femtosecond-pulse laser and handheld probe," *J. Biophotonics* **4**(1–2), 34–39 (2011).

**Benjamin Cromeey** is a PhD candidate at the University of Arizona, College of Optical Sciences. He graduated as valedictorian with his BS degree in optical sciences and engineering from the University of Arizona in 2015. He is a member of SPIE.

**Ashley McDaniel** is a chemical engineering student/researcher at the University of Arizona.

**Terry Matsunaga** is a research professor in medical imaging and biomedical engineering at the University of Arizona. He received his AB degree in biochemistry from the University of California, Berkeley, and his PharmD in clinical pharmacy and PhD in pharmaceutical chemistry from the University of California, San Francisco. He also trained as a clinical pharmacy resident at the University of Michigan and National Institute of Health (NIH) postdoctoral fellow in chemistry at the University of Arizona.

**Josef Vagner** is the director of the Ligand Discovery Lab, the University of Arizona. He received his BS and MS degrees in organic chemistry from the Institute of Technology, Prague, and his doctorate in pharmaceutical chemistry from the Institute of Pharmacology and Biochemistry, Prague, in 1990.

**Khanh Quoc Kieu** is a tenure-tracked assistant professor at the College of Optical Sciences. He received his BS degree in applied physics, his MS degree in laser technologies from Institute of Fine Mechanics and Optics University, St. Petersburg, Russia, and his PhD in optical sciences from the College of Optical Sciences in 2007.

**Bhaskar Banerjee** obtained his medical degree from the University of London, United Kingdom. He is a board-certified gastroenterologist and a professor of medicine at the College of Medicine, University of Arizona, with joint appointments at the College of Optical Sciences and Department of Biomedical Engineering. His research interest is in the development of innovative optical imaging techniques and devices.